Journal of Heat Transfer. Received January 29, 2021;
Accepted manuscript posted May 15, 2021. doi:10.1115/1.4051187

A multiscale method for coupled steady-state heat conduction and radiative transfer equations in composite materials

Zi-Xiang Tong[a], Ming-Jia Li*[b], Yi-Si Yu[b], Jing-Yu Guo[b]

[a] *School of Human Settlements and Civil Engineering, Xi'an Jiaotong University, Xi'an, Shaanxi, 710049, China*

[b] *Key Laboratory of Thermo-Fluid Science and Engineering of Ministry of Education, School of Energy & Power Engineering, Xi'an Jiaotong University, Xi'an, Shaanxi, 710049, China*

*Corresponding author email: mjli1990@xjtu.edu.cn

Abstract

Predictions of coupled conduction-radiation heat transfer processes in periodic composite materials are important for applications of the materials in high-temperature environments. The homogenization method is widely used for the heat conduction equation, but the coupled radiative transfer equation is seldom studied. In this work, the homogenization method is extended to the coupled conduction-radiation heat transfer in composite materials with periodic microscopic structures, in which both the heat conduction equation and the radiative transfer equation are analyzed. Homogenized equations are obtained for the macroscopic heat transfer. Unit cell problems are also derived, which provide the effective coefficients for the homogenized equations and the local temperature and radiation corrections. A second-order asymptotic expansion of the temperature field and a first-order asymptotic expansion of the radiative intensity field are established. A multiscale numerical algorithm is proposed to simulate the coupled conduction-radiation heat transfer in composite materials. According to the numerical examples in this work,

Journal of Heat Transfer. Received January 29, 2021;
Accepted manuscript posted May 15, 2021. doi:10.1115/1.4051187

compared with the fully-resolved simulations, the relative errors of the multiscale model are less than 13% for the temperature and less than 8% for the radiation. The computational time can be reduced from more than 300 hours to less than 30 minutes. Therefore, the proposed multiscale method maintains the accuracy of the simulation and significantly improves the computational efficiency. It can provide both the average temperature and radiation fields for engineering applications and the local information in microstructures of composite materials.

Keywords: conduction-radiation heat transfer; homogenization; multiscale simulation; radiative transfer equation; composite material

Nomenclature

C	solution of the unit cell problem for the second-order temperature T_2, m^2 K/W
G	incident radiation, W/m^2
I	radiative intensity, W/m^2
K_{ij}	effective thermal conductivity tensor, W/m K
k_{ij}^{ε}	thermal conductivity tensor, W/m K
$M_{\alpha\beta}$	solution of the unit cell problem for the second-order temperature T_2, m^2
N_{α}	solution of the unit cell problem for the first-order temperature T_1, m
$\mathbf{n}$	outward unit normal
T	temperature, K
w_i	weights in the discrete ordinate method
X	macroscopic structure domain

Journal of Heat Transfer. Received January 29, 2021;
Accepted manuscript posted May 15, 2021. doi:10.1115/1.4051187

$\mathbf{x}$	$\mathbf{x} = (x_1, x_2, x_3)$ macroscopic coordinate of the structure
$\lvert Y \rvert$	volume of the unit cell, m^3
$\mathbf{y}$	$\mathbf{y} = (y_1, y_2, y_3)$ microscopic coordinate of the unit cell

Greek Letters

α^ε	absorption coefficient, /m
$\overline{\alpha}$	effective absorption coefficient, /m
β^ε	extinction coefficient, /m
$\overline{\beta}$	effective extinction coefficient, /m
Γ	boundary of the domain
ε	ratio of the scales between the macroscopic and microscopic coordinates
σ^ε	scattering coefficient, /m
$\overline{\sigma\Phi}$	effective product of the scattering coefficient and the phase function, /m
σ_B	Stefan-Boltzmann constant, 5.67×10^{-8} W/m^2 K^4
Φ^ε	scattering phase function
ϕ	volume fraction
Ω	$\Omega = (\Omega_1, \Omega_2, \Omega_3)$ unit vector of a radiation direction

Subscripts and Superscripts

0	homogenized value
1	first-order correction
2	second-order correction
b	boundary
F	fully-resolved simulation

Journal of Heat Transfer. Received January 29, 2021;
Accepted manuscript posted May 15, 2021. doi:10.1115/1.4051187

i, j	component of a vector or tensor
M	multiscale simulation
ref	reference value
α, β	component of a vector or tensor

1. Introduction

Composite materials and porous materials are widely used in high-temperature environments due to their special mechanical and thermal properties. For example, ceramic matrix composites and silica aerogels are used in propulsion systems and thermal protection systems of aerospace vehicles [1-3]. Ceramic foams are used as absorbers of volumetric solar air receivers [4-5]. Predictions of heat transfer processes in these materials are important for their applications. There are two difficulties in the predictions. Firstly, composite materials and porous materials have complex microscopic structures. The local thermal properties fluctuate according to the structures. Secondly, effects of the thermal radiation become important in high-temperature environments. Traditionally, correlations for effective thermal properties are used in these problems, which are obtained from theoretical analyses or experiments [3,6]. The correlations usually depend on the specific structures of the materials and their utilizations are limited. Also, microscopic temperature fluctuations are neglected. In order to accurately predict the thermal performances of composite materials, a multiscale model for the coupled conduction-radiation heat transfer problem is needed [7-8].

Homogenization methods are widely used for analyses of mechanical and thermal properties of composite materials [9-11]. Although homogenization analyses of the heat conduction are well established, homogenization analyses of the coupled conduction-radiation heat transfer still need

Journal of Heat Transfer. Received January 29, 2021;
Accepted manuscript posted May 15, 2021. doi:10.1115/1.4051187

further studies. Some researchers considered the heat radiation in their homogenization analyses. In the existing researches, the heat radiation was treated as a separate heat transfer process, a radiative boundary condition or a heat source in the heat conduction equation. For example, in the multiscale model proposed by Liu and Zhang [12], the heat conduction and radiation equations were solved separately. A homogenization method was firstly applied to the heat conduction equation to obtain the effective conductive thermal conductivity and the temperature field in a unit cell. Then, the effective radiative thermal conductivity was calculated based on the temperature field in the unit cell. Some researches on the multiscale heat transfer in porous media included radiation boundary conditions in the pores. For example, Allaire and El Ganaoui [13] proposed a two-scale homogenization model for heat transfer problems in periodically perforated materials with a radiation boundary condition in the perforations. In the model, the radiative boundary condition was multiplied by a scaling factor ε^{-1} and the solution of the temperature field was expanded to the first order of ε. Yang et al. [14] developed a second-order two-scale method for steady-state heat transfer problems in porous media with interior surface radiations. The original radiation boundary condition without the scaling factor was used. The solution of the temperature was expanded to the second order of ε. The model was extended into transient heat transfer problems [15] and porous materials with three different length scales [16]. The convective heat transfer in the pores was further included in the above models [17-19]. Haymes and Gal [20] used a similar model to study the multiscale heat transfer in porous building materials. Moreover, Huang and Cao [21-22] conducted a homogenization analysis of the transient heat transfer with radiation effects. In their model, the heat radiation was considered as a volumetric heat source, which was proportional to T^4, in the heat conduction equation.

Journal of Heat Transfer. Received January 29, 2021;
Accepted manuscript posted May 15, 2021. doi:10.1115/1.4051187

In the above researches, multiscale analyses were mainly applied to the heat conduction equation. Radiation effects were treated as boundary conditions or volumetric heat sources. The radiative transfer equation was not included in the analyses. Meanwhile, homogenizations of the radiative transfer equation was studied in some researches. For example, Mathiaud and Salvarani [23] proposed a homogenization method for transport problems with highly oscillatory coefficients. The derived numerical model was applied to the radiative transfer equation. Homogenizations of linear Boltzmann equation were studied by Goudon and Mellet [24] and Hutridurga et al. [25]. The radiative transfer equation was a special form of the Boltzmann equation. However, the heat conduction was not within the scope of these researches.

In this work, the homogenization method will be extended to heat transfer problems with both the heat conduction equation and the radiative transfer equation. Both the temperature field and the radiative intensity field will be considered. The rest of the paper is organized as follows. In Section 2, the homogenization analysis will be applied to the coupled heat conduction and radiative transfer equations. Homogenized equations, unit cell problems and expressions of effective coefficients will be obtained. A multiscale numerical model will be presented in Section 3. In Section 4, the proposed multiscale model will be validated by numerical examples. Finally, some conclusions are summarized in Section 5.

2. Homogenization of Heat Conduction and Radiative Transfer Equations

The problem in this work is sketched in Fig. 1. The coupled conduction and radiation heat transfer occurs in a composite material with periodic local structures. The unit cell is the smallest unit that repetitively constitutes the composite material. There are two scales in this problem, which are the macroscale of the material and the microscale of the unit cell. The coordinate in the macroscale is

Journal of Heat Transfer. Received January 29, 2021;
Accepted manuscript posted May 15, 2021. doi:10.1115/1.4051187

denoted by **x** and the coordinate in the unit cell is denoted by **y**. Because the characteristic length of the unit cell is much smaller than that of the macroscale, the ratio between **x** and **y** is denoted by a small parameter ε, which means $\mathbf{y}=\mathbf{x}/\varepsilon$ [9]. Based on the homogenization analysis in this section, homogenized equations will be derived for the heat transfer in macroscale. A set of unit cell problems will also be obtained to provide the effective thermal conductivity and radiation coefficients for the homogenized equations, as well as the supplementary temperature and radiation corrections in the unit cells.

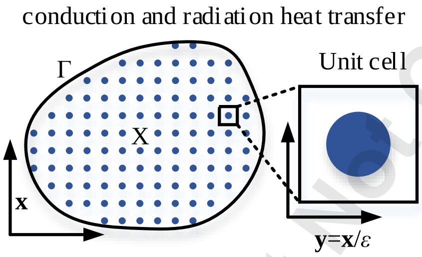

Fig. 1 A sketch of the problem in this work

The analysis starts from the governing equations of the steady-state conduction-radiation heat transfer [26]:

$$\frac{\partial}{\partial x_i}\left(k_{ij}^{\varepsilon}(\mathbf{x})\frac{\partial T^{\varepsilon}(\mathbf{x})}{\partial x_j}\right)-\alpha^{\varepsilon}(\mathbf{x})\left(4\sigma_{\mathrm{B}}\left[T^{\varepsilon}(\mathbf{x})\right]^4-\int_{4\pi}I^{\varepsilon}(\mathbf{x},\Omega)\mathrm{d}\Omega\right)=0,\quad \mathbf{x}\in \mathrm{X} \tag{1}$$

$$\begin{aligned}\Omega_i\frac{\partial I^{\varepsilon}(\mathbf{x},\Omega)}{\partial x_i}&=-\beta^{\varepsilon}(\mathbf{x})I^{\varepsilon}(\mathbf{x},\Omega)+\frac{\sigma_{\mathrm{B}}}{\pi}\alpha^{\varepsilon}(\mathbf{x})\left[T^{\varepsilon}(\mathbf{x})\right]^4\\&+\frac{1}{4\pi}\sigma^{\varepsilon}(\mathbf{x})\int_{4\pi}I^{\varepsilon}(\mathbf{x},\Omega')\Phi^{\varepsilon}(\mathbf{x},\Omega',\Omega)\mathrm{d}\Omega',\quad \mathbf{x}\in \mathrm{X}\end{aligned} \tag{2}$$

The boundary conditions are:

$$\begin{cases}T^{\varepsilon}(\mathbf{x})=T_{\mathrm{b}}(\mathbf{x}), & \mathbf{x}\in\Gamma\\ I^{\varepsilon}(\mathbf{x},\Omega)=\dfrac{\sigma_{\mathrm{B}}}{\pi}T_{\mathrm{b}}^4(\mathbf{x}), & \text{for }\Omega\cdot\mathbf{n}<0,\ \mathbf{x}\in\Gamma\end{cases} \tag{3}$$

Equation (1) is the heat conduction equation, where the $T^{\varepsilon}(\mathbf{x})$ is the temperature and the **x** represents the position vector (x_1, x_2, x_3). The X represents the whole computational domain. The k_{ij}^{ε} is the symmetric thermal conductivity tensor of the material. Equation (2) is the radiative transfer

Journal of Heat Transfer. Received January 29, 2021;
Accepted manuscript posted May 15, 2021. doi:10.1115/1.4051187

equation, which describes the radiative intensity $I^\varepsilon(\mathbf{x}, \Omega)$ along the direction Ω. The Ω_i is the ith cosine of the unit vector of direction Ω. The α^ε, β^ε and σ^ε are the absorption, extinction and scattering coefficients, which have the relation $\beta^\varepsilon=\alpha^\varepsilon+\sigma^\varepsilon$. The $\Phi^\varepsilon(\mathbf{x}, \Omega', \Omega)$ is the scattering phase function, which describes the angular distribution of the scattered radiative intensity. The Stefan-Boltzmann constant σ_B is 5.67×10^{-8} W·m^{-2}·K^{-4}. As for the boundary conditions on Γ, the Dirichlet boundary condition for the temperature is considered in this work. The radiation boundary is assumed to be black, and the inlet radiative intensity is calculated by the black body radiation.

In the homogenization analysis, the temperature and the radiative intensity are expanded into the following series of the small parameter ε [9]:

$$T^\varepsilon(\mathbf{x}) = T_0(\mathbf{x},\mathbf{y}) + \varepsilon T_1(\mathbf{x},\mathbf{y}) + \varepsilon^2 T_2(\mathbf{x},\mathbf{y}) + O(\varepsilon^3) \tag{4}$$

$$I^\varepsilon(\mathbf{x},\Omega) = I_0(\mathbf{x},\mathbf{y},\Omega) + \varepsilon I_1(\mathbf{x},\mathbf{y},\Omega) + O(\varepsilon^2) \tag{5}$$

It should be mentioned that $\mathbf{y}=\mathbf{x}/\varepsilon$. The thermal conductivities and the radiation coefficients fluctuate in the unit cell according to the materials, so the k_{ij}^ε, α^ε, β^ε, σ^ε and Φ^ε are all functions of $\mathbf{y}$.

The $(T^\varepsilon)^4$ can be represented by:

$$\left[T^\varepsilon(\mathbf{x})\right]^4 = T_0^4 + \varepsilon\left(4T_0^3T_1\right) + \varepsilon^2\left(6T_0^2T_1^2 + 4T_0^3T_2\right) + O(\varepsilon^3) \tag{6}$$

The spatial derivative is given by [9]:

$$\frac{\partial}{\partial x_i} = \frac{\partial}{\partial x_i} + \frac{1}{\varepsilon}\frac{\partial}{\partial y_i} \tag{7}$$

The above expansions are substituted into Eqs. (1) and (2), and the equations in different orders of ε can be obtained.

In the order of ε^{-2}, there is only one equation for the heat conduction:

$$\frac{\partial}{\partial y_i}\left(k_{ij}^\varepsilon(\mathbf{y})\frac{\partial T_0(\mathbf{x},\mathbf{y})}{\partial y_j}\right) = 0 \tag{8}$$

Therefore, the T_0 is independent of $\mathbf{y}$ and is only a function of $\mathbf{x}$:

Journal of Heat Transfer. Received January 29, 2021;
Accepted manuscript posted May 15, 2021. doi:10.1115/1.4051187

$$T_0 = T_0(\mathbf{x}) \tag{9}$$

In the order of ε^{-1}, the heat conduction and radiative transfer equations are:

$$\frac{\partial}{\partial x_i}\left(k_{ij}^{\varepsilon}(\mathbf{y})\frac{\partial T_0(\mathbf{x})}{\partial y_j}\right)+\frac{\partial}{\partial y_i}\left(k_{ij}^{\varepsilon}(\mathbf{y})\frac{\partial T_0(\mathbf{x})}{\partial x_j}+k_{ij}^{\varepsilon}(\mathbf{y})\frac{\partial T_1(\mathbf{x},\mathbf{y})}{\partial y_j}\right)=0 \tag{10}$$

$$\Omega_i\frac{\partial I_0(\mathbf{x},\mathbf{y},\Omega)}{\partial y_i}=0 \tag{11}$$

Equation (11) also demonstrates that the I_0 is not a function of $\mathbf{y}$:

$$I_0 = I_0(\mathbf{x},\Omega) \tag{12}$$

Based on Eq. (9), Eq. (10) can be simplified as:

$$\frac{\partial}{\partial y_i}\left(k_{ij}^{\varepsilon}(\mathbf{y})\frac{\partial T_1(\mathbf{x},\mathbf{y})}{\partial y_j}\right)=-\frac{\partial}{\partial y_i}\left(k_{ij}^{\varepsilon}(\mathbf{y})\frac{\partial T_0(\mathbf{x})}{\partial x_j}\right) \tag{13}$$

According to the form of Eq. (13), it can be assumed that the T_1 is expressed as:

$$T_1(\mathbf{x},\mathbf{y}) = N_i(\mathbf{y})\frac{\partial T_0(\mathbf{x})}{\partial x_i} \tag{14}$$

By substituting Eq. (14) into Eq. (13), the unit cell problem for $N_\alpha(\mathbf{y})$ can be obtained:

$$\begin{cases}\dfrac{\partial}{\partial y_i}\left(k_{ij}^{\varepsilon}(\mathbf{y})\dfrac{\partial N_\alpha(\mathbf{y})}{\partial y_j}\right)=-\dfrac{\partial k_{i\alpha}^{\varepsilon}(\mathbf{y})}{\partial y_i}\\ N_\alpha(\mathbf{y})\ \text{ is periodic in Y}\end{cases} \tag{15}$$

Next, the heat conduction and radiative transfer equations in the order of ε^0 are:

$$\frac{\partial}{\partial x_i}\left(k_{ij}^{\varepsilon}\frac{\partial T_0}{\partial x_j}\right)+\frac{\partial}{\partial x_i}\left(k_{ij}^{\varepsilon}\frac{\partial T_1}{\partial y_j}\right)+\frac{\partial}{\partial y_i}\left(k_{ij}^{\varepsilon}\frac{\partial T_1}{\partial x_j}\right)+\frac{\partial}{\partial y_i}\left(k_{ij}^{\varepsilon}\frac{\partial T_2}{\partial y_j}\right)-4\alpha^{\varepsilon}\sigma_{\mathrm{B}}T_0^{\,4}+\alpha^{\varepsilon}\int_{4\pi}I_0\,\mathrm{d}\Omega=0 \tag{16}$$

$$\Omega_i\left(\frac{\partial I_0}{\partial x_i}+\frac{\partial I_1}{\partial y_i}\right)=-\beta^{\varepsilon}I_0+\frac{\alpha^{\varepsilon}\sigma_{\mathrm{B}}}{\pi}T_0^{\,4}+\frac{\sigma^{\varepsilon}}{4\pi}\int_{4\pi}I_0(\mathbf{x},\Omega')\Phi^{\varepsilon}(\mathbf{y},\Omega',\Omega)\,\mathrm{d}\Omega' \tag{17}$$

Then, the macroscopic homogenized heat conduction and radiative transfer equations can be obtained by taking volumetric averages of Eqs. (16) and (17) in the unit cell.

The homogenized heat conduction equation is the volumetric average of Eq. (16):

Journal of Heat Transfer. Received January 29, 2021;
Accepted manuscript posted May 15, 2021. doi:10.1115/1.4051187

$$\begin{cases} \dfrac{\partial}{\partial x_i}\left(K_{ij}\dfrac{\partial T_0}{\partial x_j}\right) - 4\bar{\alpha}\sigma_{\mathrm{B}}T_0^{\,4} + \bar{\alpha}\int_{4\pi} I_0 \mathrm{d}\Omega = 0, \quad \mathbf{x}\in \mathrm{X} \\ T_0(\mathbf{x}) = T_{\mathrm{b}}(\mathbf{x}), \quad \mathbf{x}\in \Gamma \end{cases} \tag{18}$$

where the effective thermal conductivity K_{ij} and the effective absorption coefficient $\bar{\alpha}$ are given by:

$$K_{ij} = \frac{1}{|Y|}\int\left(k_{ij}^{\varepsilon}(\mathbf{y}) + k_{ip}^{\varepsilon}(\mathbf{y})\frac{\partial N_j(\mathbf{y})}{\partial y_p}\right)\mathrm{d}\mathbf{y} \tag{19}$$

$$\bar{\alpha} = \frac{1}{|Y|}\int \alpha^{\varepsilon}(\mathbf{y})\mathrm{d}\mathbf{y} \tag{20}$$

The terms $\dfrac{\partial}{\partial y_i}\left(k_{ij}^{\varepsilon}\dfrac{\partial T_1}{\partial x_j}\right)$ and $\dfrac{\partial}{\partial y_i}\left(k_{ij}^{\varepsilon}\dfrac{\partial T_2}{\partial y_j}\right)$ are eliminated because the T_1 and T_2 are periodic in the unit cell.

The homogenized radiative transfer equation is the volumetric average of Eq. (17):

$$\begin{cases} \Omega_i\dfrac{\partial I_0}{\partial x_i} = -\bar{\beta}I_0 + \dfrac{\bar{\alpha}\sigma_{\mathrm{B}}}{\pi}T_0^{\,4} + \dfrac{1}{4\pi}\int_{4\pi} I_0(\mathbf{x},\Omega')\overline{\sigma\Phi}(\Omega',\Omega)\mathrm{d}\Omega', \quad \mathbf{x}\in \mathrm{X} \\ I_0(\mathbf{x},\Omega) = \dfrac{\sigma_{\mathrm{B}}}{\pi}T_{\mathrm{b}}^{4}(\mathbf{x}), \ \text{ for } \Omega\cdot\mathbf{n}<0, \ \mathbf{x}\in \Gamma \end{cases} \tag{21}$$

where the effective extinction coefficient and the effective product of scattering coefficient and phase function are calculated by:

$$\bar{\beta} = \frac{1}{|Y|}\int \beta^{\varepsilon}(\mathbf{y})\mathrm{d}\mathbf{y} \tag{22}$$

$$\overline{\sigma\Phi}(\Omega',\Omega) = \frac{1}{|Y|}\int \sigma^{\varepsilon}(\mathbf{y})\Phi^{\varepsilon}(\mathbf{y},\Omega',\Omega)\mathrm{d}\mathbf{y} \tag{23}$$

In this derivation, it is unnecessary to assume that the I_1 is periodic in the unit cell. It is only assumed that:

$$\left\langle \Omega_i\frac{\partial I_1}{\partial y_i}\right\rangle = \frac{1}{|Y|}\int\frac{\partial(\Omega_i I_1)}{\partial y_i}\mathrm{d}\mathbf{y} = \frac{1}{|Y|}\int \Omega_i I_1 n_i \mathrm{d}S = 0 \tag{24}$$

where n_i is the outward pointing unit normal and dS is the surface element of the unit cell. Equation (24) means that there is no net source of I_1 in the unit cell.

The higher ordered temperature and radiation fields can be obtained by subtracting the

Journal of Heat Transfer. Received January 29, 2021;
Accepted manuscript posted May 15, 2021. doi:10.1115/1.4051187

homogenized equations from Eqs. (16) and (17). Subtracting Eq. (18) from Eq. (16) and using Eq. (14), the following equation is obtained:

$$\begin{aligned}&\left(k_{ij}^{\varepsilon}-K_{ij}+k_{ip}^{\varepsilon}\frac{\partial N_j}{\partial y_p}+\frac{\partial\left(k_{pi}^{\varepsilon}N_j\right)}{\partial y_p}\right)\frac{\partial^2 T_0}{\partial x_i\partial x_j}+\frac{\partial}{\partial y_i}\left(k_{ij}^{\varepsilon}\frac{\partial T_2}{\partial y_j}\right)\\&-\left(\alpha^{\varepsilon}-\bar{\alpha}\right)\left(4\sigma_{\mathrm{B}}T_0^{\,4}-\int_{4\pi}I_0\mathrm{d}\Omega\right)=0\end{aligned}\tag{25}$$

According to the form of Eq. (25), it can be assumed that the T_2 is expressed as:

$$T_2\left(\mathbf{x},\mathbf{y}\right)=M_{\alpha\beta}\left(\mathbf{y}\right)\frac{\partial^2 T_0\left(\mathbf{x}\right)}{\partial x_\alpha\partial x_\beta}+C\left(\mathbf{y}\right)\left(4\sigma_{\mathrm{B}}T_0^{\,4}-\int_{4\pi}I_0\mathrm{d}\Omega\right)\tag{26}$$

Thus, Eq. (25) is equivalent to the following two unit cell problems:

$$\begin{cases}\dfrac{\partial}{\partial y_i}\left(k_{ij}^{\varepsilon}\dfrac{\partial M_{\alpha\beta}\left(\mathbf{y}\right)}{\partial y_j}\right)=-\left(k_{\alpha\beta}^{\varepsilon}-K_{\alpha\beta}+k_{\alpha i}^{\varepsilon}\dfrac{\partial N_\beta}{\partial y_i}+\dfrac{\partial\left(k_{\alpha i}^{\varepsilon}N_\beta\right)}{\partial y_i}\right)\\ M_{\alpha\beta}\left(\mathbf{y}\right)\ \text{ is periodic in Y}\end{cases}\tag{27}$$

$$\begin{cases}\dfrac{\partial}{\partial y_i}\left(k_{ij}^{\varepsilon}\dfrac{\partial C\left(\mathbf{y}\right)}{\partial y_j}\right)=\alpha^{\varepsilon}-\bar{\alpha}\\ C\left(\mathbf{y}\right)\ \text{ is periodic in Y}\end{cases}\tag{28}$$

It should be mentioned that the periodic boundary conditions in Eqs. (15), (27) and (28) are not sufficient to provide unique solutions for the unit cell problems. In practice, it is also required that the volumetric averages of N_α, $M_{\alpha\beta}$ and C are zero in the unit cell. Thus, the unit-cell averages of T_1 and T_2 also vanish. This is consistent with the definition that the T_0 is the macroscopic average temperature.

Finally, the governing equation for I_1 can be obtained by subtracting Eq. (21) from Eq. (17):

$$\Omega_i\frac{\partial I_1}{\partial y_i}=-\left(\beta^{\varepsilon}-\bar{\beta}\right)I_0+\frac{\left(\alpha^{\varepsilon}-\bar{\alpha}\right)\sigma_{\mathrm{B}}}{\pi}T_0^{\,4}+\frac{1}{4\pi}\int_{4\pi}I_0\left(\mathbf{x},\Omega'\right)\left(\sigma^{\varepsilon}\Phi^{\varepsilon}-\overline{\sigma\Phi}\right)\mathrm{d}\Omega'\tag{29}$$

It can be seen that the I_1 in Eq. (29) satisfies Eq. (24). Equation (29) depends on the average radiative intensity I_0 and the temperature T_0. Therefore, Eq. (29) varies in different unit cells and the I_1 should be solved in each unit cell. In this work, two different boundary conditions for I_1 are

Journal of Heat Transfer. Received January 29, 2021;
Accepted manuscript posted May 15, 2021. doi:10.1115/1.4051187

considered. The first is similar to the boundary conditions of N_α, $M_{\alpha\beta}$ and C. It is assumed that:

$$I_1 \text{ is periodic in each unit cell} \tag{30}$$

The second is that:

$$I_1 \text{ is solved in the whole domain with } I_1(\mathbf{x},\Omega)=0, \text{ for } \Omega\cdot\mathbf{n}<0, \ \mathbf{x}\in\Gamma \tag{31}$$

Boundary condition (31) means that the solutions of I_1 in the upstream unit cells provide the inlet boundary conditions of I_1 for the downstream unit cells. Because the right-hand-side of Eq. (29) does not contain I_1, iterations in each unit cell are not necessary if there is no periodic boundary condition in the whole domain. The accuracy of the two boundary conditions will be compared in the numerical examples in Section 4.2.

When the T_0, T_1, T_2, I_0 and I_1 are obtained, the approximated temperature field and radiative intensity field can be reconstructed by:

$$T^\varepsilon = T_0 + \varepsilon T_1 + \varepsilon^2 T_2 = T_0 + \varepsilon N_i \frac{\partial T_0}{\partial x_i} + \varepsilon^2 \left[M_{\alpha\beta} \frac{\partial^2 T_0}{\partial x_\alpha \partial x_\beta} + C\left(4\sigma_{\mathrm{B}} T_0^{\,4} - \int_{4\pi} I_0 \mathrm{d}\Omega\right)\right] \tag{32}$$

$$I^\varepsilon = I_0 + \varepsilon I_1 \tag{33}$$

3. Numerical Algorithm

A multiscale numerical algorithm is proposed based on the analysis in Section 2. The computational procedure is shown in Fig. 2, which contains the following steps.

1) Identify the geometry of the unit cell and build meshes for both the unit cell problem and the macroscopic problem.

2) Solve Eq. (15) in the unit cell and obtain $N_\alpha(\mathbf{y})$. Calculate the effective thermal conductivity, the effective absorption and extinction coefficient and the effective product of scattering coefficient and phase function by Eqs. (19), (20), (22) and (23).

3) Solve the homogenized Eqs (18) and (21) to obtain the macroscopic $T_0(\mathbf{x})$ and $I_0(\mathbf{x})$.

Journal of Heat Transfer. Received January 29, 2021;
Accepted manuscript posted May 15, 2021. doi:10.1115/1.4051187

4) Solve Eqs. (27), (28) and (29) to obtain $M_{\alpha\beta}(\mathbf{y})$, $C(\mathbf{y})$ and $I_1(\mathbf{y})$.

5) Reconstruct the temperature field T^{ε} by the combination of Eqs. (32), (14) and (26). Reconstruct the radiative intensity field I^{ε} by Eq. (33).

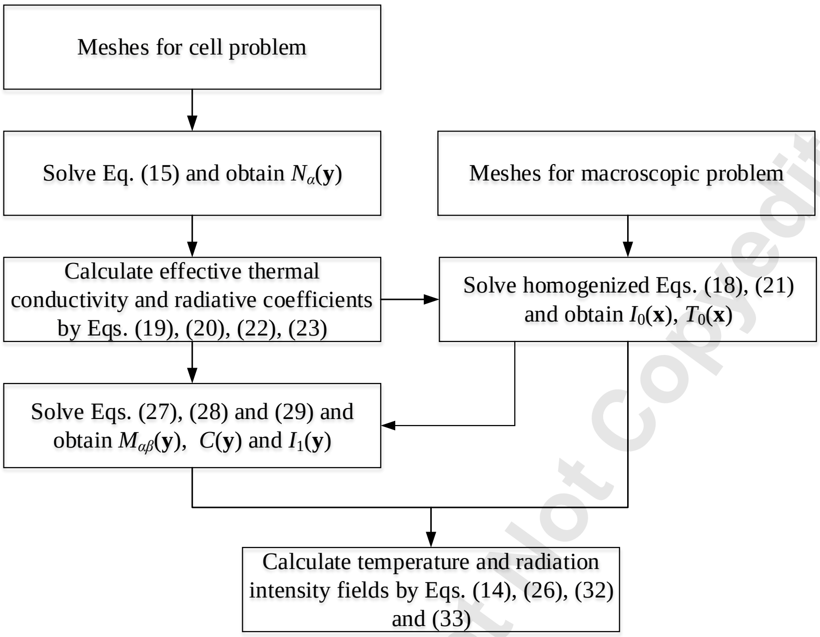

Fig. 2 The computational procedure of the multiscale numerical model

The Cartesian meshes are employed in this work. The material in each control volume is specified and the corresponding thermal properties are determined based on the material. The finite volume method (FVM) is used to solve Eqs. (15), (18), (27) and (28), which are related to the heat conduction equation [27]. The discrete ordinate method (DOM) is used to solve Eqs. (21) and (29), which are related to the radiative transfer equation [26]. For the 2D problems in this work, the S6 DOM with 24 discrete directions is used [26].

In the FVM, the thermal conductivities on the interfaces of a control volume are the harmonic mean values of the thermal conductivities in the neighboring control volumes. The volume integral is conducted in each control volume to derive discrete equations. Therefore, the FVM contains only first-order derivatives. The finite differences are used to calculate the first-order derivatives.

Journal of Heat Transfer. Received January 29, 2021;
Accepted manuscript posted May 15, 2021. doi:10.1115/1.4051187

However, the calculation of T_2 in Eq. (26) contains second-order partial derivatives of T_0. The second-order finite difference of T_0 can be adopted. For example, if the coordinate **x** is expressed by (x_1, x_2) in 2D simulations, the derivative $\left.\frac{\partial^2 T_0}{\partial {x_1}^2}\right|_{i,j}$ at a node (i, j) can be calculated by:

$$\left.\frac{\partial^2 T_0}{\partial {x_1}^2}\right|_{i,j} = \frac{T_{0,i+1,j} - 2T_{0,i,j} + T_{0,i-1,j}}{\Delta x^2} \tag{34}$$

where $T_{0,i,j}$ is the T_0 at the node (i, j). However, in practice it is found that the finite difference Eq. (34) has large fluctuations in the computational domain and will lead to large errors in the reconstructed temperature fields. Therefore, the second-order derivatives are calculated by the least square method. For each node (i, j), the coordinates and the T_0 of 7×7 neighboring nodes (i+m, j+n), m, n=-3~3, are used to fit a quadric surface by the least square method. The quadric surface is expressed as:

$$T_0\left(x_1, x_2\right) = a_{11}x_1^2 + a_{12}x_1x_2 + a_{22}x_2^2 + b_1x_1 + b_2x_1 + c \tag{35}$$

where (x_1, x_2) is the coordinate and a_{11}, a_{12}, a_{22}, b_1, b_2, c are the fitted parameters. Then, the second-order derivatives of T_0 can be obtained by:

$$\left.\frac{\partial^2 T_0}{\partial {x_1}^2}\right|_{i,j} = 2a_{11},\quad \left.\frac{\partial^2 T_0}{\partial {x_2}^2}\right|_{i,j} = 2a_{22},\quad \left.\frac{\partial^2 T_0}{\partial x_1 \partial x_2}\right|_{i,j} = a_{12} \tag{36}$$

In addition, it should be mentioned that although the small parameter ε is important for the analysis in Section 2, its specific value has no influence on the results of numerical simulations. It can be seen that the orders of the partial derivatives with respect to **y** on the left and right sides of Eqs. (15), (27), (28) and (29) are not equal. Because the coordinate **y** is influenced by ε according to **y**=**x**/ε, the values of N_α, $M_{\alpha\beta}$, C and I_1 are also influenced by ε. For example, it is assumed that ε_1 and ε_2 are used in two numerical simulations for a same problem, and their ratio is r=ε_2/ε_1. Then, the relation for **y** is $\mathbf{y}_2$=$\mathbf{y}_1$/r. Applying $\mathbf{y}_1$ and $\mathbf{y}_2$ in Eq. (15) respectively, it can be found that the results

Journal of Heat Transfer. Received January 29, 2021;
Accepted manuscript posted May 15, 2021. doi:10.1115/1.4051187

have a relation $N_{\alpha,2}=N_{\alpha,1}/r$, where the subscripts 1 and 2 denote the results which are corresponding to $\mathbf{y}_1$ and $\mathbf{y}_2$. Similarly, relations $M_{\alpha\beta,2}= M_{\alpha\beta,1}/r^2$, $C_2= C_1/r^2$ and $I_{1,2}=I_{1,1}/r$ can be obtained from Eqs. (27), (28) and (29). Taking into consideration $\varepsilon_2=r\varepsilon_1$, it can be found that $\varepsilon_2N_{\alpha,2}=\varepsilon_1N_{\alpha,1}$, $\varepsilon_2I_{1,2}=\varepsilon_1I_{1,1}$, $\varepsilon_2^2M_{\alpha\beta,2}=\varepsilon_1^2M_{\alpha\beta,1}$, and $\varepsilon_2^2C_2=\varepsilon_1^2C_1$. Therefore, the T^ε and I^ε calculated from Eqs. (32) and (33) are the same for both ε_1 and ε_2. In this work, if the spatial step for the homogenized macroscale simulation is Δx and the spatial step for the unit cell problem is Δy, the ε is chosen as $\varepsilon=\Delta y/\Delta x$.

4. Numerical Examples

4.1 Effective thermal conductivity

Firstly, the effective thermal conductivities calculated by Eq. (19) are compared with theoretical predictions. The unit cell is the same as that in Fig. 4. The grid size of the unit cell is 400×400, and a particle of radius R is placed in the center of the unit cell. The dimensionless parameters are used. The R changes from 10 to 140. The thermal conductivity of the base material is k_0=1, and that of the particle is k_1=5 or k_1=10. If the volume fraction of the particle is denoted by ϕ, the effective thermal conductivity K of the unit cell can be predicted by the following equation [28]:

$$\frac{K}{k_0}=1+\frac{2\phi}{\left(\frac{k_1+k_0}{k_1-k_0}\right)-\phi+\left(\frac{k_1-k_0}{k_1+k_0}\right)\left(0.30584\phi^4+0.013363\phi^8\right)} \tag{37}$$

The effective thermal conductivities predicted by Eq. (19) are compared with the values calculated from Eq. (37), and the results are shown in Fig. 3. It can be seen that the predicted thermal conductivities coincide well with that calculated from Eq. (37) for different particle volume fractions and particle thermal conductivities. Therefore, the effective thermal conductivity of the model is validated.

Journal of Heat Transfer. Received January 29, 2021;
Accepted manuscript posted May 15, 2021. doi:10.1115/1.4051187

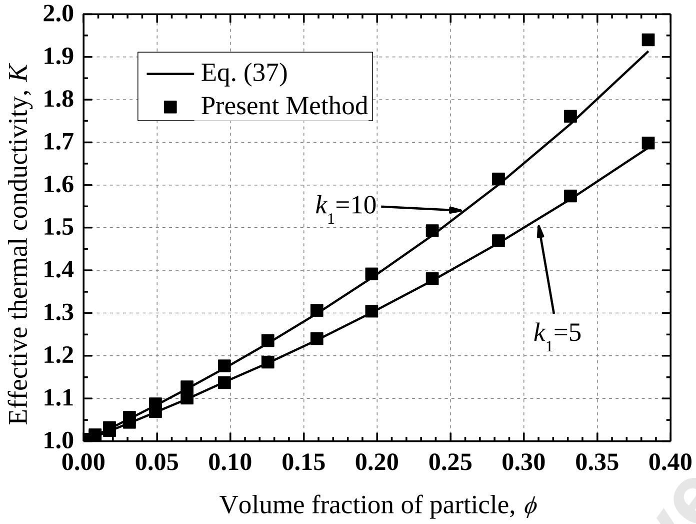

Fig. 3 The comparison between the effective thermal conductivities predicted by the multiscale model and the theoretical correlation

4.2 Example 1

In the following sections, 2D numerical examples are used to validate the proposed multiscale model. The first example is the conduction-radiation heat transfer in SiO_2 aerogel doped with TiO_2 opacifier particles. A sketch of the problem is illustrated in Fig. 4. The computational domain is composed of ten 0.1mm×0.1mm unit cells. A TiO_2 particles is placed at the center of each unit cell and the diameter of the particle is 20μm. The thermal conductivities and the absorption and scattering coefficients of the SiO_2 aerogel and the TiO_2 particle are given in Table 1. The scattering is assumed to be isotropic and $\Phi^{\varepsilon}=1$ is used. The temperature of the left boundary is 900K and the temperature of the right boundary is 500K. The periodic boundary condition is used on the other boundaries.

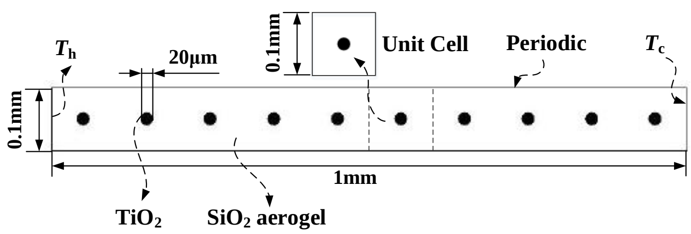

Fig. 4 The computational domain for Example 1

Table 1 Properties of the materials

Material	Thermal conductivity/ $Wm^{-1}K^{-1}$	Absorption coefficient/ m^{-1}	Scattering Coefficient/ m^{-1}
SiO_2 aerogel	0.0177	15.4	24.8
TiO_2	4.39	7208	0

The problem is solved by the proposed multiscale numerical model. In order to evaluate the accuracy of the multiscale model, a fully-resolved simulation of the problem is used as the benchmark. A grid independence test of the unit cell problem is conducted first to determine the grid size of the simulation. The grid size of the unit cell changes from 50×50 to 600×600, and the diameter of the particle is from $10\Delta x$ to $120\Delta x$, respectively. The N_α for each grid size are solved and the corresponding effective thermal conductivities are calculated. The effective thermal conductivities for different grid sizes are given in Figure S1, available in Supplemental Material, part of the ASME Digital Collection. It is found that the variation of the thermal conductivity is relatively small when the grid size is larger than 200×200. Taking into consideration the computational cost, the 200×200 mesh is adopted for the unit cell problem and the diameter of the particle is $40\Delta x$. The corresponding grid size of the fully-resolved problem is 2000×200. As for the homogenized equations, the grid size is 500×50. The thermal and radiation properties in each grid node are specified in accordance with the material in that node.

The convergence criterion for N_α, $M_{\alpha\beta}$, C, and I_1 is that the relative error E_ϕ between two successive iterations is less than 10^{-8}, which is defined as:

$$E_\phi = \sqrt{\sum_{i,j}\left(\phi_{i,j}^{n+1} - \phi_{i,j}^{n}\right)^2 \Big/ \sum_{i,j}\left(\phi_{i,j}^{n}\right)^2} \tag{38}$$

The variable ϕ represents N_α, $M_{\alpha\beta}$, or C, and the $\phi_{i,j}^{n}$ is the value at node (i, j) after nth iteration.

Journal of Heat Transfer. Received January 29, 2021;
Accepted manuscript posted May 15, 2021. doi:10.1115/1.4051187

As for the simulation of conduction and radiation heat transfer, the relative error E is defined as:

$$E=\sqrt{\sum_{i,j}\left(T_{i,j}^{n+1}-T_{i,j}^{n}\right)^2\Big/\sum_{i,j}\left(T_{i,j}^{n}-T_{\mathrm{ref}}\right)^2}+\sqrt{\sum_{i,j,k}\left(I_{i,j,k}^{n+1}-I_{i,j,k}^{n}\right)^2\Big/\sum_{i,j,k}\left(I_{i,j,k}^{n}-I_{\mathrm{ref}}\right)^2} \tag{39}$$

where the k represents the kth direction of the DOM. The reference temperature is $T_{\mathrm{ref}}=(T_{\mathrm{h}}+T_{\mathrm{c}})/2$ and the reference radiative intensity is $I_{\mathrm{ref}}=\sigma_{\mathrm{B}}T_{\mathrm{ref}}^4/\pi$. The convergence criterion is $E<10^{-8}$.

Incident radiations G are shown in the figures of this paper instead of the individual radiative intensities I_i. In DOM, the G is calculated by $G=\sum_k w_k I_k$, where the w_k are the weights of the discrete directions [26].

The solutions of N_α, $M_{\alpha\beta}$ and C in the unit cell are shown in Fig. 5. Because of the symmetric structure of the unit cell, the effective thermal conductivity is isotropic and the value is 0.0218 $\mathrm{Wm^{-1}K^{-1}}$ according to the solution of N_α. The effective absorption coefficient and scattering coefficient are 242.7$\mathrm{m^{-1}}$ and 24.02$\mathrm{m^{-1}}$. These parameters are used in Eqs. (18) and (21) to calculate the homogenized temperature and radiative intensity fields, which are shown in Fig. 6 (b) and Fig. 7 (b) separately. Then, the multiscale temperature field can be reconstructed and the result is given in Fig. 6 (c). The relative errors of the temperature and radiative intensity fields are defined as:

$$E_T=\sqrt{\sum_{i,j}\left(T_{i,j}^{\varepsilon}-T_{i,j}^{\mathrm{F}}\right)^2\Big/\sum_{i,j}\left(T_{i,j}^{\mathrm{F}}-T_{\mathrm{ref}}\right)^2},\quad E_I=\sqrt{\sum_{i,j,k}\left(I_{i,j,k}^{\varepsilon}-I_{i,j,k}^{\mathrm{F}}\right)^2\Big/\sum_{i,j,k}\left(I_{i,j,k}^{\mathrm{F}}-I_{\mathrm{ref}}\right)^2} \tag{40}$$

where the superscripts ε and F represent the multiscale results and the fully-resolved results, respectively. The relative errors of the homogenized temperature T_0 and the reconstructed multiscale temperature T^ε are 0.90% and 0.48%.

Journal of Heat Transfer. Received January 29, 2021;
Accepted manuscript posted May 15, 2021. doi:10.1115/1.4051187

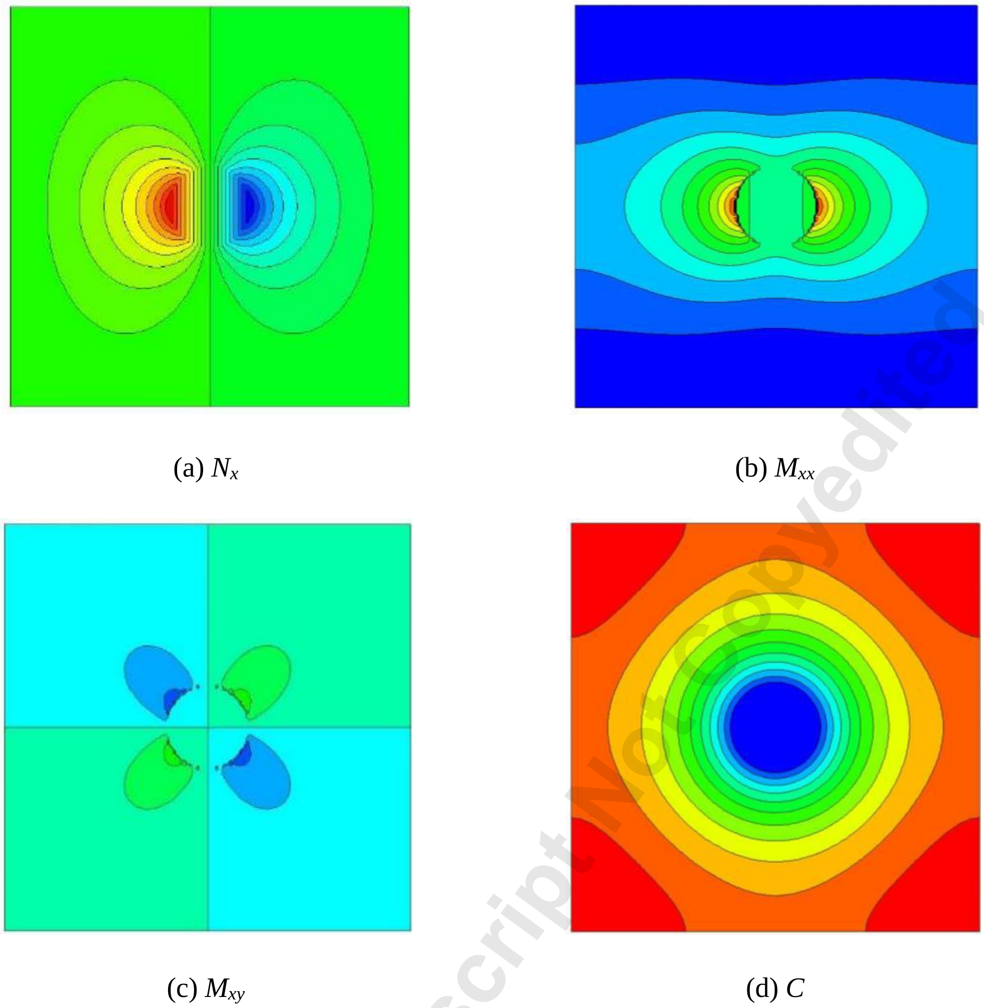

Fig. 5 The results of N_α, $M_{\alpha\beta}$ and C in the unit cell for Example 1

Then, the multiscale radiative intensity fields are reconstructed. The T_0 is used in Eq. (29) to calculate I_1, and the boundary conditions (30) and (31) for I_1 are compared. The results of the reconstructed multiscale incident radiation fields G^ε are shown in Fig. 7 (c) and Fig. 7 (d). The corresponding first-order corrections G_1 are also given in Figure S2, available in Supplemental Material, part of the ASME Digital Collection. Because the I_1 in each unit cell is solved individually under the boundary condition (30), the radiative intensity is discontinuous between different unit cells and the discontinuity is more significant near the left boundary. In addition, the periodic boundary condition for I_1 in the individual unit cell leads to large fluctuations near the four corners of the unit cell. The result with the boundary condition (31) is smoother because the I_1 is solved in

Journal of Heat Transfer. Received January 29, 2021;
Accepted manuscript posted May 15, 2021. doi:10.1115/1.4051187

the whole domain. Finally, the reconstructed multiscale incident radiations are compared with the result of the fully-resolved simulation. The relative error of I_0 is 12%, but the relative error of I^ε with boundary condition (30) is 19%, which is even higher. On the contrary, the relative error of I^ε with boundary condition (31) drops to 7.3%. The relative errors of I^ε in each individual unit cell are also calculated and shown in Table 2. It can be seen that with the boundary condition (31), the error of I^ε in each unit cell is reduced. With boundary condition (30), the relative errors in all the unit cells are large because of the fluctuations near the corners. In conclusion, boundary condition (31) is better than boundary condition (30). Therefore, boundary condition (31) will be chosen in the following simulations of this work, and the I_1 will be solved in the whole domain.

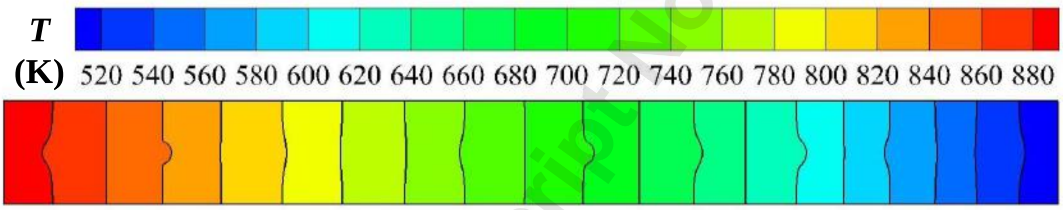

(a) Fully-resolved temperature

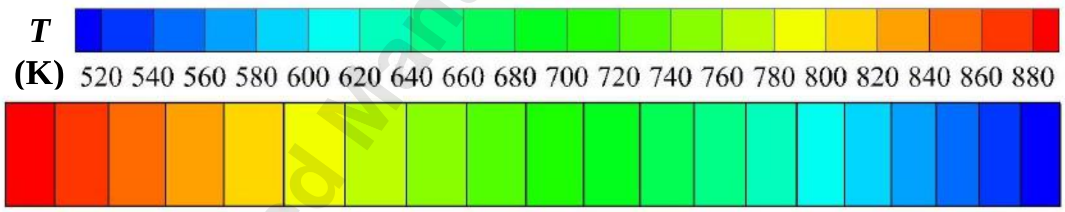

(b) Homogenized temperature

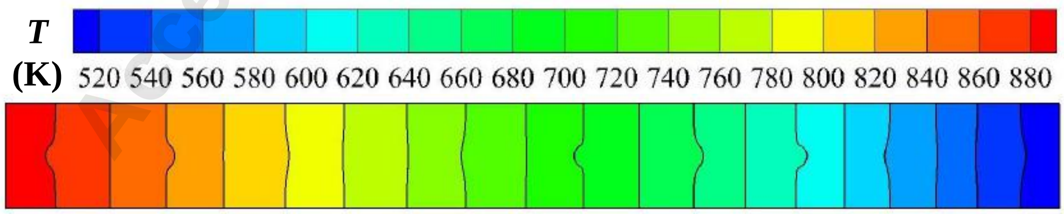

(c) Reconstructed multiscale temperature

Fig. 6 The temperature fields for Example 1

Journal of Heat Transfer. Received January 29, 2021;
Accepted manuscript posted May 15, 2021. doi:10.1115/1.4051187

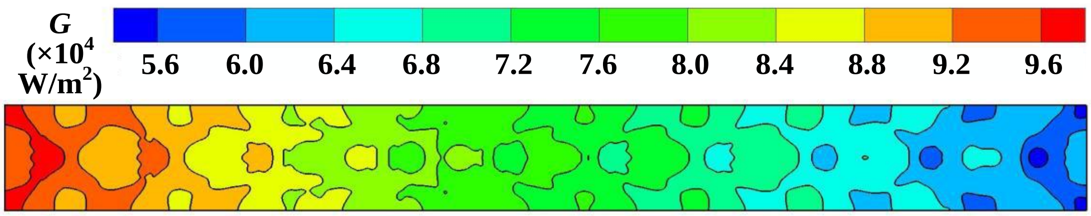

(a) Fully-resolved incident radiation

(b) Homogenized incident radiation

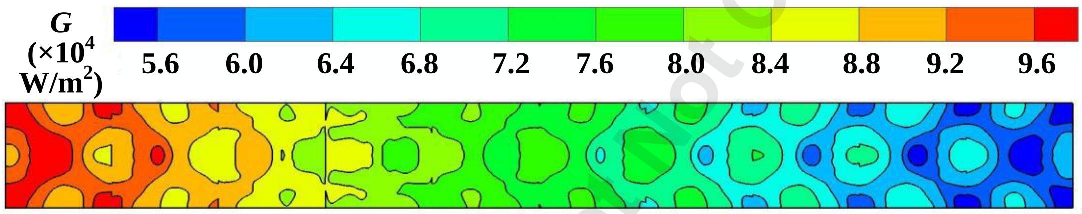

(c) Reconstructed multiscale incident radiation with boundary condition (30)

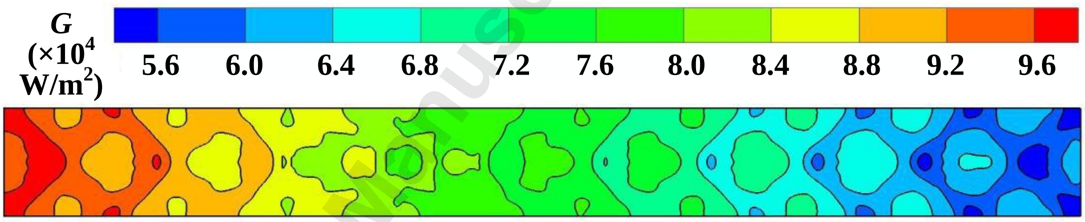

(d) Reconstructed multiscale incident radiation with boundary condition (31)

Fig. 7 The incident radiation fields for Example 1

Table 2 Relative errors of I^ε in each unit cell (%)

Unit cell	1	2	3	4	5	6	7	8	9	10
I_0	11.6	9.8	8.8	8.8	9.5	10.9	12.8	14.9	17.1	19.4
I^ε with boundary condition (30)	19.8	19.1	19.3	19.6	19.7	19.6	19.4	19.2	19.0	18.9

Journal of Heat Transfer. Received January 29, 2021;
Accepted manuscript posted May 15, 2021. doi:10.1115/1.4051187

I^ε with boundary condition (31)	6.7	5.4	4.5	4.1	4.6	5.8	7.5	9.3	11.3	13.3

Finally, as for the CPU time, the fully-resolved simulation takes 84229s (23.4h) to reach the 10^{-8} convergence criterion. Using the same computer resources, the multiscale simulation consumes 1641s (27.4 min) in total with boundary condition (30) for I_1, which includes 98.2s for N_α, 234.5s for $M_{\alpha\beta}$, 70.7s for C, 476.7s for the homogenized conduction-radiation equations, 19.0s for the reconstruction of the multiscale temperature field, and 742.1s for the calculation of I_1 and the reconstruction of the radiative intensity field. In addition, the boundary condition (31) consumes only 130.5s for the I_1 and the reconstruction of the radiation field, which is more efficient. The reason is that this boundary condition prevents the iteration in each individual unit cell, compared with the boundary condition (30). Therefore, the proposed multiscale model can significantly improve the efficiency of the simulation and maintain the accuracy.

4.3 Example 2

Example 2 is similar to example 1, but the computational domain is composed of 7×7 unit cells, and the temperatures of the up and bottom boundaries are specified as T_c, as shown in Fig. 8. The solutions of the unit cell problems are the same as those in Fig. 5. The temperature fields and the incident radiation fields of the fully-resolved simulation and the multiscale simulation are given in Fig. 9 and Fig. 10. For the calculation of I_1, the boundary condition (31) is used. It can be seen that the multiscale numerical model can reproduce the local temperature and radiation fluctuations caused by the TiO_2 particles.

The relative error of the homogenized temperature field is 1.57%, and that of the reconstructed

Journal of Heat Transfer. Received January 29, 2021;
Accepted manuscript posted May 15, 2021. doi:10.1115/1.4051187

second-order temperature field is 0.93%. It should be mentioned that the relative error of the first-order temperature field (T_0+εT_1) is only 0.66%, which is even lower. The reason is that the second-order derivatives near the top-left and bottom-left corners have large fluctuations due to the steep temperature gradient. The errors in each unit cell are also compared. It is found that the second-order temperature has lower errors except in the unit cells near the top-left and bottom-left corners. The plots of the errors are given in Figure S3, available in Supplemental Material, part of the ASME Digital Collection. These errors near the corners result in a higher error of the overall temperature field. As for the radiation field, the error of the homogenized radiation field is 10.6% and the error of the reconstructed multiscale radiation field drops to 6.6%. In addition, the computational time is reduced from 238.9h to 15.6min.

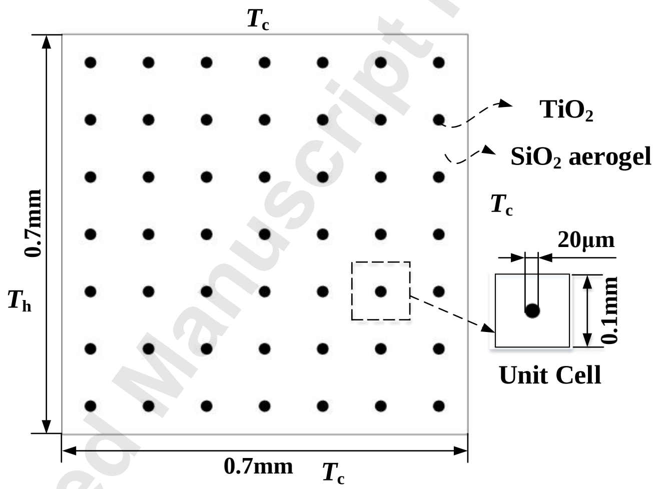

Fig. 8 The computational domain for Example 2

Journal of Heat Transfer. Received January 29, 2021;
Accepted manuscript posted May 15, 2021. doi:10.1115/1.4051187

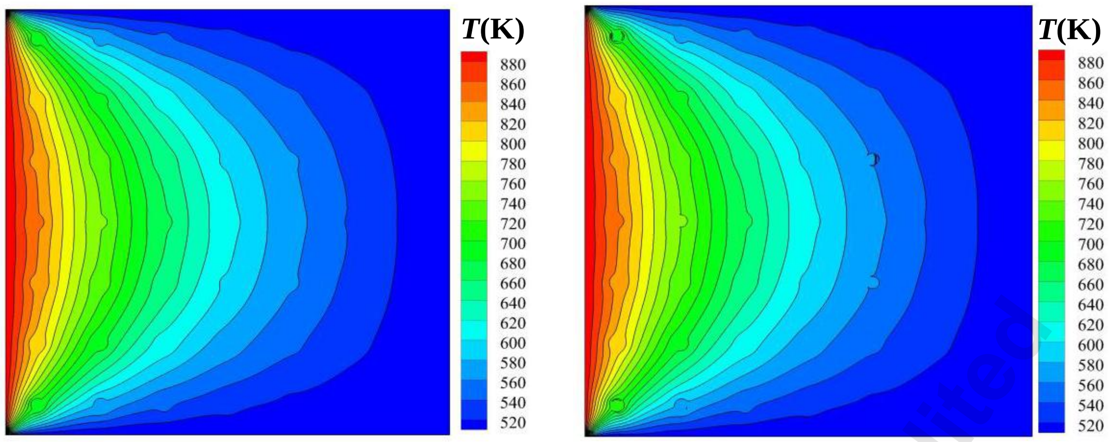

(a) Fully-resolved temperature (b) Reconstructed multiscale temperature

Fig. 9 The temperature fields for Example 2

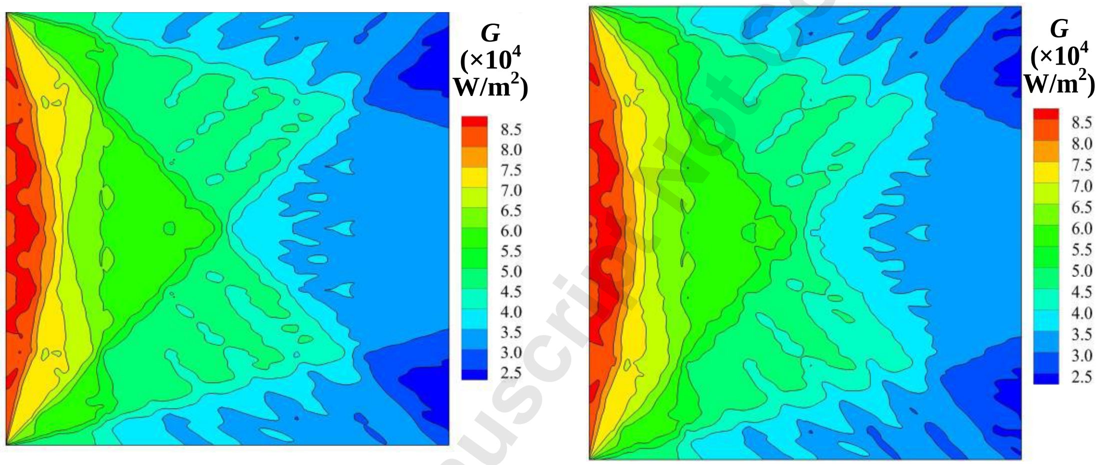

(a) Fully-resolved incident radiation (b) Reconstructed multiscale incident radiation

Fig. 10 The incident radiation fields for Example 2

4.4 Example 3

In this example, anisotropic structures are generated by changing the circular TiO_2 particle in example 2 into elliptical particles. The lengths of the major axis and the minor axis of the elliptical particle are 95μm and 9μm. The particles are either horizontally aligned or 45° tilted, as shown in Fig. 11.

Journal of Heat Transfer. Received January 29, 2021;
Accepted manuscript posted May 15, 2021. doi:10.1115/1.4051187

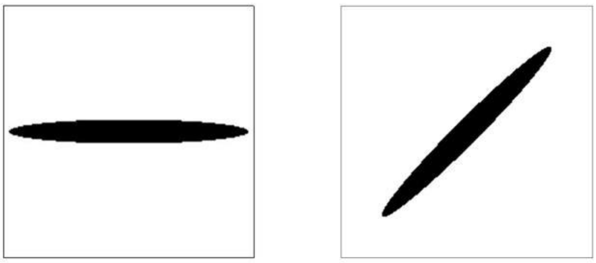

horizontally aligned particle tilted particle

Fig. 11 The unit cells for Example 3

For the horizontally aligned particle, the solution of N_α in the unit cell provides an effective thermal conductivity tensor:

$$K_{ij} = \begin{bmatrix} 0.0567 & 0 \\ 0 & 0.0301 \end{bmatrix} \mathrm{Wm^{-1}K^{-1}} \tag{41}$$

The tensor demonstrates that the heat conduction along the x-direction is stronger than that along the y-direction because the high-thermal-conductivity TiO_2 particle is elongated along the x-direction. The temperature and incident radiation fields of the fully-resolved simulation and the multiscale simulation are given in Fig. 12 and Fig. 13, respectively. The relative errors of the temperature and radiation fields are 12.4% and 5.6%. In addition, the multiscale numerical model reduces the computational time from 314.6h to 21.0min.

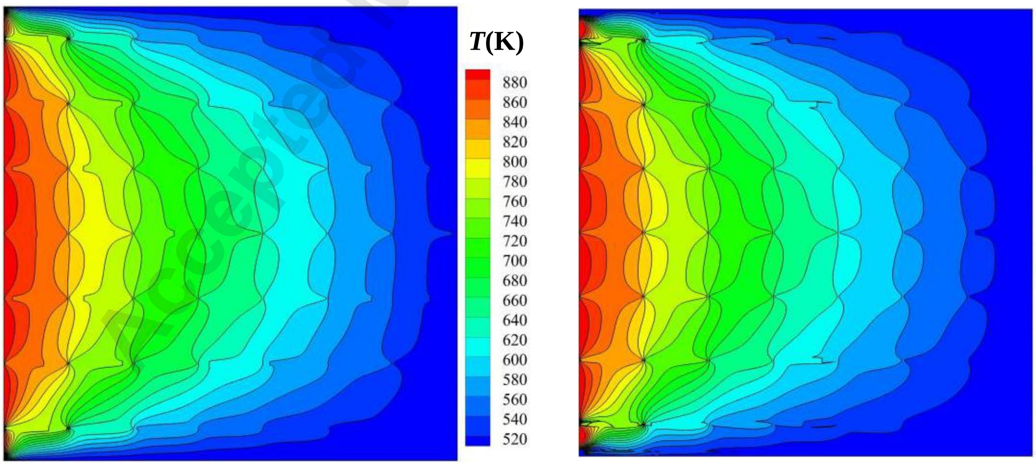

(a) Fully-resolved temperature (b) Reconstructed multiscale temperature

Fig. 12 The temperature fields for Example 3 with horizontally aligned particles

Journal of Heat Transfer. Received January 29, 2021;
Accepted manuscript posted May 15, 2021. doi:10.1115/1.4051187

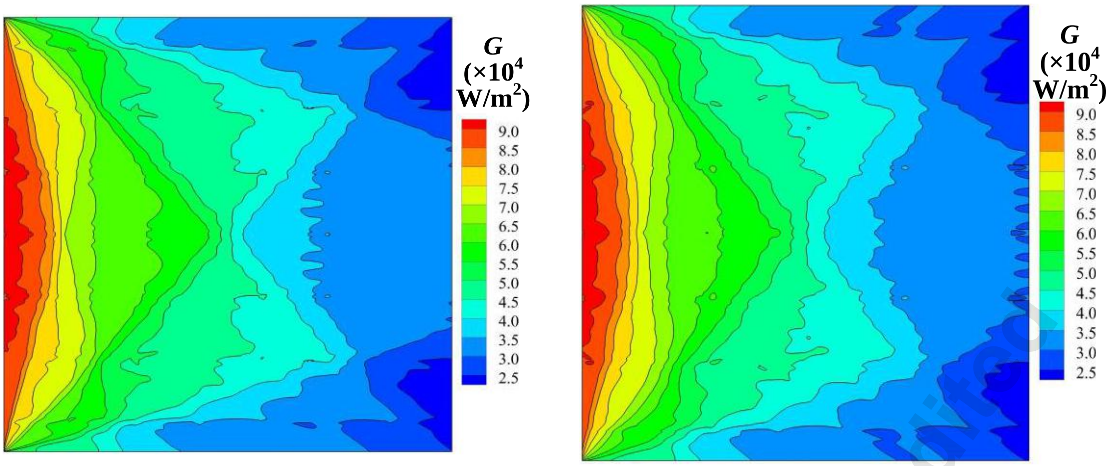

(a) Fully-resolved incident radiation (b) Reconstructed multiscale incident radiation

Fig. 13 The incident radiation fields for Example 3 with horizontally aligned particles

As for the tiled particle, the effective thermal conductivity tensor calculated from the unit cell problem is:

$$K_{ij} = \begin{bmatrix} 0.0343 & 0.0067 \\ 0.0067 & 0.0343 \end{bmatrix} \mathrm{Wm^{-1}K^{-1}} \tag{42}$$

It can be found that the principal directions of the thermal conductivity are 45° and 135°, which are consistent with the structure of the unit cell. The corresponding principal values of the thermal conductivity are 0.0410 $\mathrm{Wm^{-1}K^{-1}}$ and 0.0276 $\mathrm{Wm^{-1}K^{-1}}$. The simulation results of the temperature and incident radiation fields are given in Fig. 14 and Fig. 15. The relative errors of the temperature and radiation fields are 10.1% and 3.0%. The computational time of the multiscale simulation is 14.7min while the fully-resolved simulation costs 364h. Finally, it can be seen that the multiscale simulation can reproduce the anisotropic effects of the elliptical particles in this problem. It can provide the detailed temperature and radiation information in the local structures and save the computational time.

Journal of Heat Transfer. Received January 29, 2021;
Accepted manuscript posted May 15, 2021. doi:10.1115/1.4051187

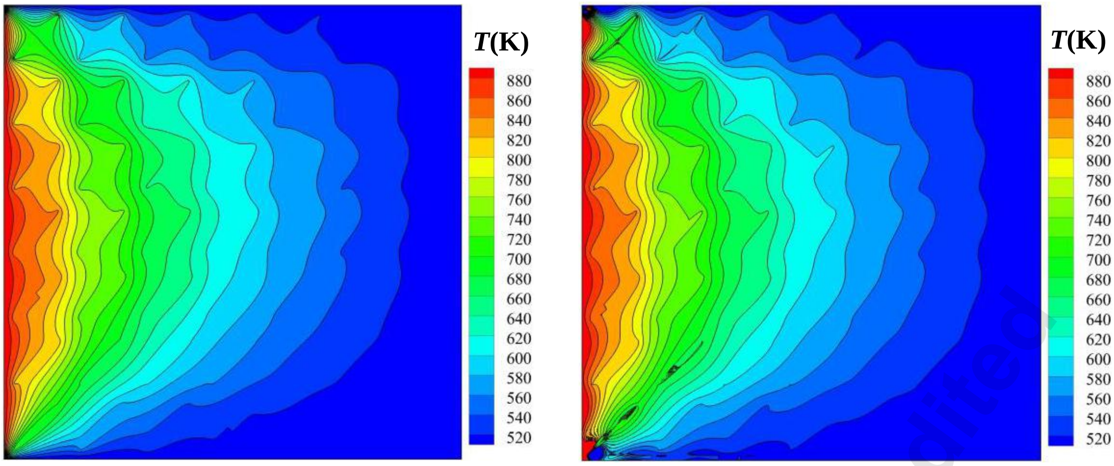

(a) Fully-resolved temperature (b) Reconstructed multiscale temperature

Fig. 14 The temperature fields for Example 3 with tilted particles

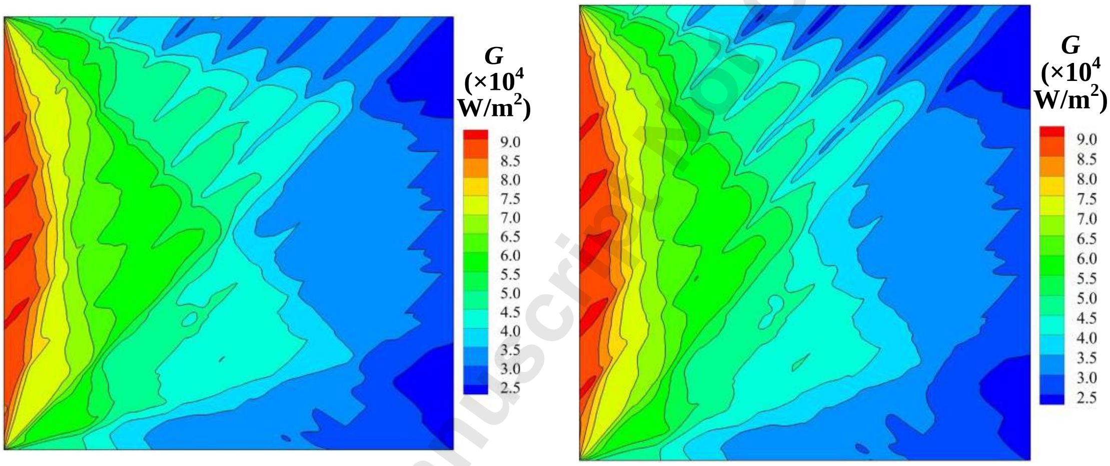

(a) Fully-resolved incident radiation (b) Reconstructed multiscale incident radiation

Fig. 15 The incident radiation fields for Example 3 with tilted particles

5. Conclusions

In the above sections, the homogenization analysis has been extended to the steady-state heat conduction and radiative transfer equations. Both the macroscopic homogenized equations and the unit cell problems are obtained. The multiscale algorithm is also proposed for the coupled conduction-radiation heat transfer problems in periodic composite materials. The main conclusions are as follows.

Journal of Heat Transfer. Received January 29, 2021;
Accepted manuscript posted May 15, 2021. doi:10.1115/1.4051187

1) The macroscopic homogenized heat conduction and radiative transfer equations have the same forms as the traditional equations. The effective thermal conductivity is related to the solution of N_α in the unit cell. As for the radiation, the effective absorption and extinction coefficients and the effective product of scattering coefficient and phase function are the volumetric averages of the corresponding coefficients in the unit cell.

2) The analysis provides a second-order approximation of the temperature field and a first-order approximation of the radiative intensity field, which can be reconstructed from the results of the homogenized equations and the unit cell problems.

3) The heat transfer processes in the SiO_2 aerogel doped with TiO_2 particles are simulated by the proposed multiscale method. It is demonstrated that the method can be used in both the isotropic and anisotropic unit cell geometries. The reconstructed temperature and radiative intensity fields can reproduce the local fluctuations due to the microscale structures.

4) Compared with the results of the fully-resolved simulations, the multiscale method can provide accurate temperature and radiative intensity fields, and can significantly increase the efficiency of the simulations.

5) It is also found that for the unit cell problem of radiative transfer, solving I_1 in the whole domain can provide better multiscale radiation results than solving I_1 in each unit cell individually with periodic boundary condition.

As for applications of the model, microscale visualization methods such as the X-ray computed tomography or the scanning electron microscope can be used to reconstruct unit cells of composite materials [5]. The thermal conductivities and radiation coefficients can be obtained from experiments or existing literature. Then, the proposed method is used to model the coupled

Journal of Heat Transfer. Received January 29, 2021;
Accepted manuscript posted May 15, 2021. doi:10.1115/1.4051187

conduction-radiation heat transfer in the materials.

The present research extends the homogenization of heat conduction equation into the coupled heat conduction and radiative transfer equations. Further researches are still needed to improve the proposed multiscale method. Some of the considerations are as follows.

1) The present analysis focuses on the steady-state conduction and radiation heat transfer problems with constant thermal properties. The unit cell problems of the temperature need to be solved only once during multiscale simulations. When the multiscale model is used in unsteady problems with temperature-related material properties, the unit cell problems need to be repetitively solved under different temperatures. The speed-up of the multiscale method should be further studied.

2) To calculate I_1 in a whole domain is inconvenient for applications because a fully-resolved mesh is needed. More researches on the boundary conditions of the unit cell problems for I_1 should be carried out.

3) Although the T_0 satisfies the boundary condition Eq. (3), the T_1 and T_2 will introduce errors to the boundary. Therefore, the present asymptotic expansion of T^ε does not exactly satisfy the boundary condition. In order to solve this problem, boundary layer solutions should be included in the future [17,21,22].

Funding Data

This study is supported by the National Natural Science Foundation of China (No. 51906186, 52076161).

The authors would also like to thank the National Numerical Windtunnel Project of China (NNW2018-ZT2A04).

Journal of Heat Transfer. Received January 29, 2021;
Accepted manuscript posted May 15, 2021. doi:10.1115/1.4051187

Reference

[1] Pichon, T., Barreteau R., Soyris P., Foucault A., Parenteau J. M., Prel Y., and Guedron S., 2009, "CMC thermal protection system for future reusable launch vehicles: Generic shingle technological maturation and tests," Acta Astronautica 65(1-2), pp. 165-176.

[2] Tang, S., and Hu, C., 2017, "Design, preparation and properties of carbon fiber reinforced ultra-high temperature ceramic composites for aerospace applications: a review," Journal of Materials Science & Technology, 33(2), pp. 117-130.

[3] He, Y.L., and Xie, T., 2015, "Advances of thermal conductivity models of nanoscale silica aerogel insulation material," Applied Thermal Engineering, 81, pp. 28-50.

[4] Wu, Z., Caliot, C., Flamant, G., and Wang, Z., 2011, "Coupled radiation and flow modeling in ceramic foam volumetric solar air receivers," Solar Energy, 85(9), pp. 2374-2385.

[5] Du, S., Tong, Z.X., Zhang, H.H., and He, Y.L., 2019, "Tomography-based determination of Nusselt number correlation for the porous volumetric solar receiver with different geometrical parameters," Renewable Energy, 135, pp. 711-718.

[6] Boomsma, K., and Poulikakos, D., 2001, "On the effective thermal conductivity of a three-dimensionally structured fluid-saturated metal foam," International Journal of Heat and Mass Transfer, 44(4), pp. 827-836.

[7] Tong, Z.X., He, Y.L., Tao, W.Q., 2019, "A review of current progress in multiscale simulations for fluid flow and heat transfer problems: The frameworks, coupling techniques and future perspectives," International Journal of Heat and Mass Transfer, 137, pp. 1263-1289.

[8] He Y.L., Tao W.Q., 2015, "Numerical Solutions of Nano/ Microphenomena Coupled With Macroscopic Process of Heat Transfer and Fluid Flow: A Brief Review," JOURNAL OF HEAT

Journal of Heat Transfer. Received January 29, 2021;
Accepted manuscript posted May 15, 2021. doi:10.1115/1.4051187

TRANSFER-TRANSACTIONS OF THE ASME, 137(9), pp. 090801.

[9] Bensoussan, A., Lions, J.L., and Papanicolaou, G., 1978, *Asymptotic analysis for periodic structures*, North-Holland Pub. Co., Amsterdam, Netherlands.

[10] Cioranescu, D., and Donato, P., 1999, *An introduction to homogenization*, Oxford University Press, Oxford, UK.

[11] Fish. J., 2014, *Practical multiscaling*, John Wiley & Sons.

[12] Liu, S., and Zhang, Y., 2006, "Multi-scale analysis method for thermal conductivity of porous material with radiation," Multidiscipline Modeling in Materials and Structures, 2(3), pp. 327-344.

[13] Allaire, G., El Ganaoui, K., 2009, "Homogenization of a conductive and radiative heat transfer problem," Multiscale Modeling & Simulation, 7(3), pp. 1148-1170.

[14] Yang, Z., Cui, J., Nie, Y., and Ma, Q., 2012, "The second-order two-scale method for heat transfer performances of periodic porous materials with interior surface radiation," CMES – Computer Modeling in Engineering & Sciences, 88(5), pp. 419-442.

[15] Yang, Z., Cui, J., Sun, Y., and Ge, J., 2015, "Multiscale computation for transient heat conduction problem with radiation boundary condition in porous materials," Finite Elements in Analysis and Design, 102, pp. 7-18.

[16] Yang, Z., Sun, Y., Cui, J., Yang, Z., and Guan, T., 2018, "A three-scale homogenization algorithm for coupled conduction-radiation problems in porous materials with multiple configurations," International Journal of Heat and Mass Transfer, 125, pp. 1196-1211.

[17] Allaire, G., and Habibi, Z., 2013, "Homogenization of a conductive, convective, and radiative heat transfer problem in a heterogeneous domain," SIAM Journal on Mathematical Analysis,

Journal of Heat Transfer. Received January 29, 2021;
Accepted manuscript posted May 15, 2021. doi:10.1115/1.4051187

45(3), pp. 1136-1178.

[18] Yang, Z., Cui, J., and Ma, Q., 2014, "The second-order two-scale computation for integrated heat transfer problem with conduction, convection and radiation in periodic porous materials," Discrete & Continuous Dynamical Systems-Series B, 19(3), pp. 827-848.

[19] Yang, Z.Q., Cui, J.Z., and Li, B.W., 2014, "Second-order two-scale computations for conductive—radiative heat transfer problem in periodic porous materials," Chinese Physics B, 23(3), pp. 030203.

[20] Haymes, R., and Gal, E., 2018, "Iterative multiscale approach for heat conduction with radiation problem in porous materials," JOURNAL OF HEAT TRANSFER-TRANSACTIONS OF THE ASME, 140(8), pp. 082002.

[21] Huang, J., and Cao, L., 2014, "Global regularity and multiscale approach for thermal radiation heat transfer," Multiscale Modeling & Simulation, 12(2), pp. 694-724.

[22] Huang, J., Cao, L., and Yang, C., 2015, "A multiscale algorithm for radiative heat transfer equation with rapidly oscillating coefficients," Applied Mathematics and Computation, 266, pp. 149-168.

[23] Mathiaud, J., and Salvarani, F., 2013, "A numerical strategy for radiative transfer problems with higly oscillating opacities," Applied Mathematics and Computation, 221, pp. 249-256.

[24] Goudon, T., and Mellet, A., 2003, "Homogenization and diffusion asymptotics of the linear Boltzmann equation," ESAIM: Control, Optimisation and Calculus of Variations, 9, pp. 371-398.

[25] Hutridurga, H., Mula, O., and Salvarani, F., 2020, "Homogenization in the energy variable for a neutron transport model," Asymptotic Analysis, 117(1-2), pp. 1-25.

Journal of Heat Transfer. Received January 29, 2021;
Accepted manuscript posted May 15, 2021. doi:10.1115/1.4051187

[26] Howell, J.R., Siegel, R., and Mengüç, M.P., 2010, *Thermal radiation heat transfer*, CRC Press, Boca Raton, USA.

[27] Patankar, S., 1980, *Numerical Heat Transfer and Fluid Flow*, CRC Press, Boca Raton, USA.

[28] Bird, R.B., Stewart, W.E., and Lightfoot, E.N., 2002, *Transport Phenomena*, John Wiley & Sons, Inc, New York, USA.

Journal of Heat Transfer. Received January 29, 2021;
Accepted manuscript posted May 15, 2021. doi:10.1115/1.4051187

List of Figure Captions

Fig. 1 A sketch of the problem in this work

Fig. 2 The computational procedure of the multiscale numerical model

Fig. 3 The comparison between the effective thermal conductivities predicted by the multiscale model and the theoretical correlation

Fig. 4 The computational domain for Example 1

Fig. 5 The results of N_{α}, $M_{\alpha\beta}$ and C in the unit cell for Example 1

Fig. 6 The temperature fields for Example 1

Fig. 7 The incident radiation fields for Example 1

Fig. 8 The computational domain for Example 2

Fig. 9 The temperature fields for Example 2

Fig. 10 The incident radiation fields for Example 2

Fig. 11 The unit cells for Example 3

Fig. 12 The temperature fields for Example 3 with horizontally aligned particles

Fig. 13 The incident radiation fields for Example 3 with horizontally aligned particles

Fig. 14 The temperature fields for Example 3 with tilted particles

Fig. 15 The incident radiation fields for Example 3 with tilted particles

Figure S1 The effective thermal conductivities for different grid sizes

Figure S2 The first-order corrections of the incident radiation, G_1, for Example 1

Figure S3 The comparison between the errors of the reconstructed first-order and second-order temperatures in different unit cells (The location of the unit cell is numbered as (column, row) for convenience)

Journal of Heat Transfer. Received January 29, 2021;
Accepted manuscript posted May 15, 2021. doi:10.1115/1.4051187

List of Table Captions

Journal of Heat Transfer. Received January 29, 2021;
Accepted manuscript posted May 15, 2021. doi:10.1115/1.4051187

Supplementary Material

A multiscale method for coupled steady-state heat conduction and radiative transfer equations in composite materials

Zi-Xiang Tong[a], Ming-Jia Li*[b], Yi-Si Yu[b], Jing-Yu Guo[b]

[a] *School of Human Settlements and Civil Engineering, Xi'an Jiaotong University, Xi'an, Shaanxi, 710049, China*

[b] *Key Laboratory of Thermo-Fluid Science and Engineering of Ministry of Education, School of Energy & Power Engineering, Xi'an Jiaotong University, Xi'an, Shaanxi, 710049, China*

*Corresponding author email: mjli1990@xjtu.edu.cn

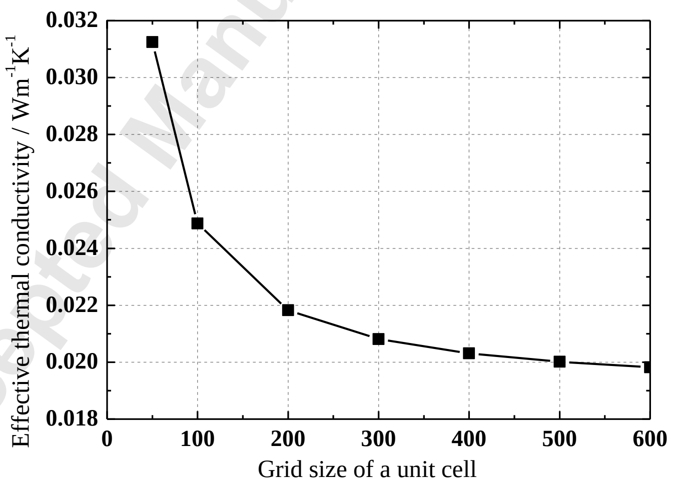

Figure S1 The effective thermal conductivities for different grid sizes

Journal of Heat Transfer. Received January 29, 2021;
Accepted manuscript posted May 15, 2021. doi:10.1115/1.4051187

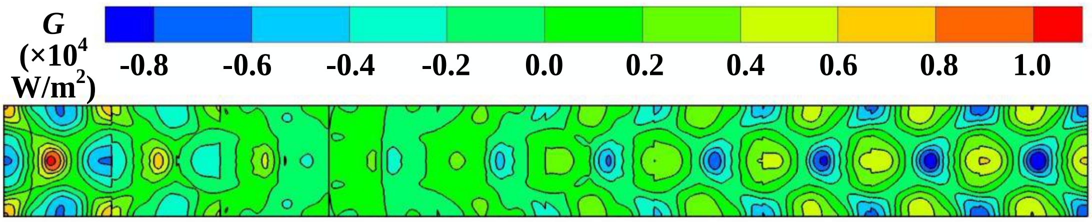

(a) Solved in individual unit cell with boundary condition (30)

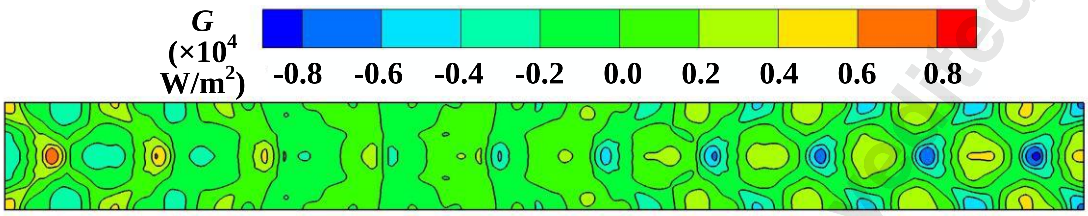

(b) Solved in the whole domain with boundary condition (31)

Figure S2 The first-order corrections of the incident radiation, G_1, for Example 1

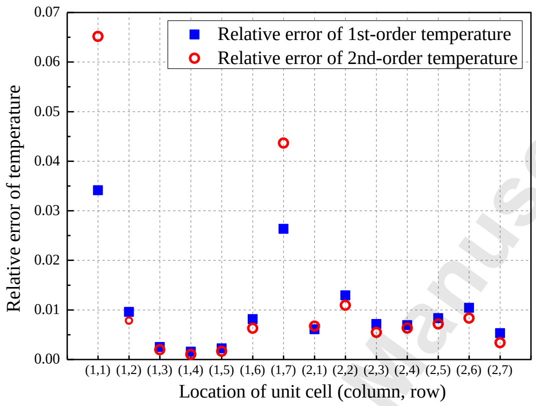

(a) Column 1~2

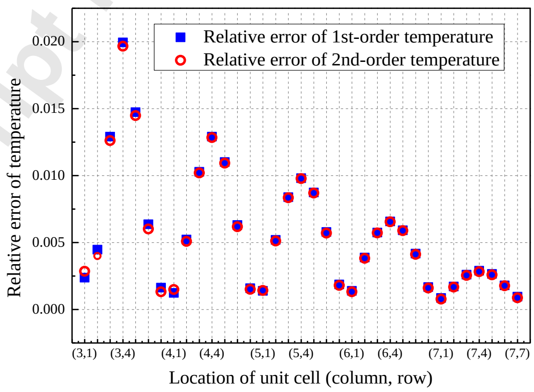

(b) Column 3~7

Figure S3 The comparison between the errors of the reconstructed first-order and second-order temperatures in different unit cells (The location of the unit cell is numbered as (column, row) for convenience)